Journal of Alloys and Compounds 509 (2011) 7778–7783

Contents lists available at ScienceDirect

Journal of Alloys and Compounds

journal homepage: www.elsevier.com/locate/jallcom

In situ synthesis of Co_3O_4/graphene nanocomposite material for lithium-ion batteries and supercapacitors with high capacity and supercapacitance

Bei Wang[a,*], Ying Wang[a], Jinsoo Park[b], Hyojun Ahn[b], Guoxiu Wang[a,*]

[a] School of Chemistry and Forensic Science, University of Technology Sydney, City Campus, Broadway, Sydney, NSW 2007, Australia
[b] School of Materials Science and Engineering, Gyeongsang National University, 900 Gazwa-dong Jinju, Gyeongnam 660-701, South Korea

ARTICLE INFO

Article history:
Received 15 February 2011
Received in revised form 27 April 2011
Accepted 27 April 2011
Available online 10 May 2011

Keywords:
Co_3O_4
Graphene
Lithium-ion batteries
Supercapacitors

ABSTRACT

Co_3O_4/graphene nanocomposite material was prepared by an *in situ* solution-based method under reflux conditions. In this reaction progress, Co^{2+} salts were converted to Co_3O_4 nanoparticles which were simultaneously inserted into the graphene layers, upon the reduction of graphite oxide to graphene. The prepared material consists of uniform Co_3O_4 nanoparticles (15–25 nm), which are well dispersed on the surfaces of graphene nanosheets. This has been confirmed through observations by field emission scanning electron microscopy, transmission electron microscopy and atomic force microscopy. The prepared composite material exhibits an initial reversible lithium storage capacity of 722 mAh g^{-1} in lithium-ion cells and a specific supercapacitance of 478 F g^{-1} in 2 M KOH electrolyte for supercapacitors, which were higher than that of the previously reported pure graphene nanosheets and Co_3O_4 nanoparticles. Co_3O_4/graphene nanocomposite material demonstrated an excellent electrochemical performance as an anode material for reversible lithium storage in lithium ion cells and as an electrode material in supercapacitors.

1. Introduction

Graphene is an allotrope of carbon atoms, which are bonded together in hexagonal sp^2 arrangement to form a two-dimensional (2D), single-layer of carbon sheets. The 2D layered graphene nanostructure shows to have ultra-high specific surface area [1–3]. The unique properties exhibited by graphene nanostructure, have attracted international research interests of its synthesis, characterizations, properties and applications. The synthetic methods of graphene derived from the classic Hummers method [4] have since been developed to suit many synthesis techniques, such as chemical vapor deposition (CVD) [5–7], electrolytic preparation [8], solvothermal and pyrolysis synthesis [9], and liquid phase exfoliation [10]. Graphene has shown to be applied as an anode material for lithium-ion batteries [11–13] and as a potential electrode material for supercapacitors [14], due to its outstanding electrochemical properties, low-cost and environmentally benign nature. The graphene composite materials comprise metal or metal oxide nanoparticles embedded between the layers of graphene nanosheets. The embedded nanoparticles have the ability to prevent graphene nanosheets from aggregation, thus maintaining the high surface area of graphene and improving their electrochemical performances. These composites therefore could have applications in lithium-ion batteries [15–17] and supercapacitors [18,19].

To date, Pt/graphene [18] and Au/graphene [20] composite materials have been prepared by chemical reduction, which resulted in metal nanoparticles depositing onto graphene layers. The synthesis of platinum and platinum–ruthenium nanoparticles supported graphene has also been reported [21]. These composites exhibited high electrocatalytic activities in the oxidation of methanol and ethanol. We have also reported the synthesis of Sn/graphene nanocomposite [22]. Sn nanoparticles (2–5 nm) were uniformly distributed onto the graphene nanosheets in a three-dimensional architecture. Our Sn/graphene nanocomposite was shown to deliver a reversible lithium storage capacity of 795 mAh g^{-1} in the second cycle with enhanced cycling stability. Nanocomposite of silicon/graphene on the other hand, was obtained from expandable graphite and reported to have even higher specific capacity of 2753 mAh g^{-1} with improved cycling capability [23]. The metal oxide/graphene nanocomposites such as SnO_2/graphene could be prepared by reassembling graphene monolayers in the presence of SnO_2 nanoparticles [15] and *in situ* chemical reduction [16]. The SnO_2/graphene nanocomposites from both methods showed to have a better lithium storage capacity and excellent cycling stability. A super-paramagnetic composite such as Fe_3O_4/graphene was produced via a chemical deposition. This product has shown to have promising applications for lithium-ion batteries and supercapacitors [24]. In the case of CuO/graphene, the material was prepared from CuO and graphene upon reduc-

* Corresponding authors. Tel.: +61 2 95141741; fax: +61 2 95141460.
E-mail addresses: Bei.Wang-1@student.uts.edu.au (B. Wang), Guoxiu.Wang@uts.edu.au (G. Wang).

0925-8388/$ – see front matter © 2011 Elsevier B.V. All rights reserved.
doi:10.1016/j.jallcom.2011.04.152

tion using hydrazine vapor [17]. The formation of TiO_2/graphene composite was reported to facilitate by SO_4^{2-} surfactants, which acted as the stabilizer of the graphene monolayers *in situ* [25]. The prepared TiO_2/graphene composite exhibited more than double the specific capacity of pure TiO_2 phase at high charge rate. Recently, we have synthesized Mn_3O_4/graphene nanocomposite with a specific capacitance of 256 F g^{-1}, almost twice the value of bare graphene nanosheets [26]. A microwave-assist reaction was reported for the synthesis of ZnO/graphene nanocomposite in an aqueous solution [19]. The composite showed to have a supercapacitance of 146 F g^{-1} with an excellent long term cycling capability.

Among the reported transition metal oxides, the cobalt (II, III) oxide (Co_3O_4) has delivered the promising electrochemical performance as an anode material for lithium-ion batteries [27] and superior specific capacitance for supercapacitors [28]. The synthesis of nanocrystalline Co_3O_4 has been carried out with various methods to obtain nanosized Co_3O_4 of different architectures, such as nanotubes [27], nanoparticles [29], nanorods [30], and hollowed spheres [31]. In the case of Co_3O_4/carbon nanotube (CNT), the nanocomposites showed to have good electrical conductivity and extra electrochemical properties, which could be potentially applicable in lithium-ion batteries [32] and supercapacitors [33].

In comparison, graphene nanosheets have a larger specific surface area, better organized 2D nanostructure, a more flexible carbon matrix and superior electrochemical properties than that of CNTs. In which case, we intent to prepare a Co_3O_4/graphene nanocomposite, by introducing Co_3O_4 nanoparticles into graphene nanosheets. Wu et al. reported an *in situ* synthesis of graphene anchored with Co_3O_4 nanoparticles in basic aqueous solution [34]. With the transformation of $Co(OH)_2$ to Co_3O_4 by calcination, Co_3O_4/graphene has been successfully obtained. In this paper, we report a new synthetic approach that involves the reduction of Co^{2+} ions from the salt solution and air-oxidation to form Co_3O_4 nanoparticles *in situ* of the graphene nanosheets. The Co_3O_4/graphene nanocomposite material will be investigated for their high electrochemical performance and potential applications as electrodes in lithium-ion batteries and supercapacitors. The individual roles and contributions of graphene and the embedded Co_3O_4 nanoparticles will also be discussed here.

2. Experimental

Graphite oxide nanosheets (GONS) were prepared using a known but modified Hummers method [4,11]. 20 ml of GONS aqueous dispersion (2 mg GONS in 1 ml of distilled water) was then obtained by ultrasonication with an ultrasonic probe (Branson Digital Sonifier S450D, 500 W, 30% amplitude) for an hour. The GONS dispersion was diluted to 80 ml with deionized water and mixed thoroughly with 20 ml of $CoCl_2$ aqueous solution (30 mg of $CoCl_2{\cdot}6H_2O$) under magnetic stirring. Graphene oxide nanosheets have carboxylic acid, epoxyl and hydroxyl functional groups on the edge and on the basal plane [35]. Therefore, individual graphene nanosheet is negatively charged [36]. Co^{2+} anions attracted and anchored on the basal planes and edges of GONS homogeneously. 20 ml of freshly prepared 5 mg ml^{-1} $NaBH_4$ solution was added dropwise within 10 min to the above solution and the mixed solution was refluxed at 100 °C for 3 h. During this process, GONS were reduced to graphene nanosheets (GNS) and Co^{2+} anions to Co nanoparticles simultaneously. The mixture was refluxed at 100 °C in the air atmosphere; Co nanoparticles were oxidized to Co_3O_4 nanoparticles rapidly. The reaction mechanism is depicted in Fig. S-1 (Supporting Information (SI)) and detailed in Ref. [22]. The resultant black precipitate was isolated by filtration, washed with deionized water and ethanol three times each, and dried under vacuum for 12 h. To increase crystallinity, the product was annealed at 200 °C under argon atmosphere for 15 h.

The X-ray diffraction (XRD) pattern of the synthesized materials was measured using a GBC MMA X-ray diffractometer. The Raman spectrum was acquired on a Jobin Yvon HR800 confocal Raman system with 632.81 nm diode laser excitation on a 300 lines/mm grating at room temperature. Field emission scanning electron microscope (FESEM) observations were performed using a JEOL JSM-7500FA FESEM instrument with the sample loaded on a carbon tape. The transmission electron microscopy (TEM) analysis was carried out using a JEOL 2011 TEM facility. Atomic force microscope (AFM) images were collected under tapping mode with a MFP-3D Stand Alone (MFD-3D-SA) AFM (manufactured by Asylum Research) with SuperSharpSilicon – Non-Contact/Tapping Mode – High Resonance Frequency – Reflex Coating (SSS-NCHR) AFM tips for enhanced resolution. The graphene (carbon) content in the composite material was determined by thermogravimetric analysis (TGA) on a Mettler Toledo TGA/DSC instrument in air at 10 °C min^{-1} at temperature range of 25–1000 °C. The specific surface area of the Co_3O_4/graphene nanocomposite was determined by the gas sorption technique using a Quanta Chrome Nova 1000 Gas Sorption Analyzer based on the Brunauer–Emmett–Teller (BET) method.

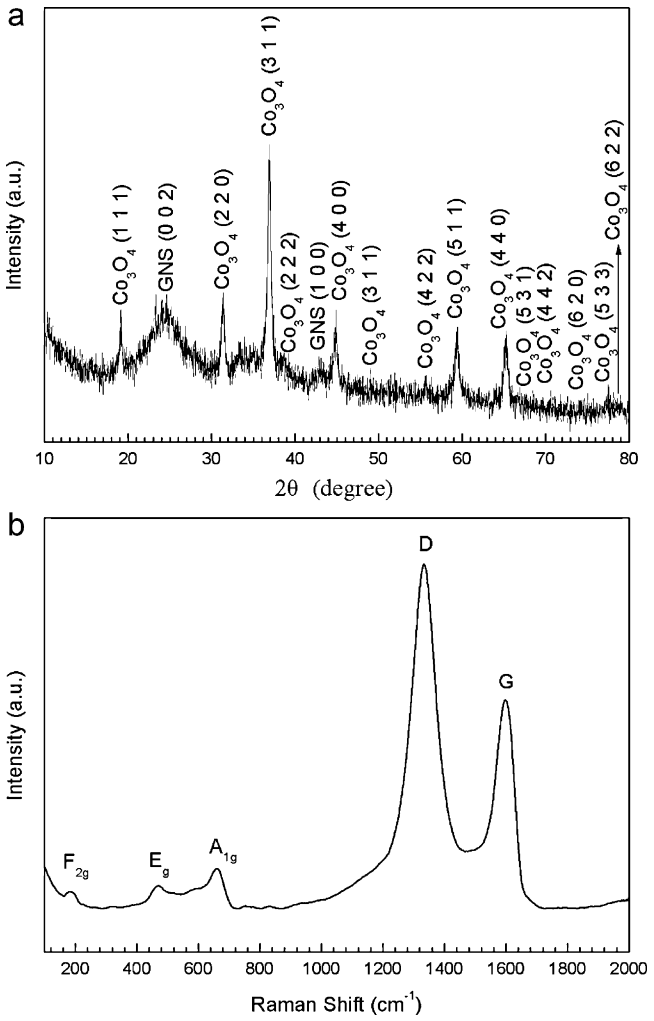

Fig. 1. (a) XRD pattern and (b) Raman spectrum of the as-prepared Co_3O_4/graphene nanocomposite material.

Electrodes for electrochemical measurements were fabricated by mixing 89.9 wt% Co_3O_4/graphene powders and 10.1 wt% polyvinylidene difluoride (PVdF) in the presence of *N*-methyl pyrrolidinone (NMP), and the resultant slurry mixture was pasted onto copper foil for lithium-ion cell test and platinum foil substrates for supercapacitor, respectively, and then heated at 110 °C under vacuum overnight. For lithium-ion batteries, CR2032-type coin cells were assembled in a glove box for electrochemical characterization. The electrolyte was 1 M $LiPF_6$ in a 1:1 mixture of ethylene carbonate and dimethyl carbonate. Li metal foil was used as the counter electrode. The cells were galvanostatically charged and discharged at a current of 55 mA, within the range of 0.01–3.0 V. Cyclic voltammetry (CV) curves were collected at 0.1 mV s^{-1} within the range of 0.01–3.0 V using an electrochemistry workstation (CHI660C). For supercapacitors, the electrochemical properties were examined by the CV technique using the CHI660C electrochemistry workstation. A beaker-type three-electrode cell was assembled with a working electrode, a counter electrode (platinum foil), and a reference electrode (saturated calomel electrode (SCE)) immersed in 2 M KOH solution. CV was applied over the potential range of −0.25 to 0.55 V in 2 M KOH, at the scan rates of 5 mV s^{-1}, 10 mV s^{-1}, 20 mV s^{-1}, and 50 mV s^{-1}, respectively. For comparative studies, the electrochemical performances of nanosized commercial Co_3O_4 powders (<50 nm, Sigma–Aldrich) and bare graphene nanosheets were investigated under the same conditions for lithium-ions batteries and supercapacitors.

3. Results and discussion

Fig. 1(a) shows the XRD pattern of the prepared Co_3O_4/graphene nanocomposite material. Well-defined diffraction peaks at around

19°, 31°, 37°, 45°, 59°, and 65° are indicative to nanosized Co_3O_4, which is in good agreement with the Joint Committee on Powder Diffraction Standards (JCPDS) card 76-1802. The sharp diffraction peaks reflect the excellent crystallinity of the Co_3O_4 nanoparticles. Graphene nanosheets (GNS) display broad graphitic (0 0 2) peak and weak (1 0 0) peak, as indicated in the XRD patterns, implying the breaking of the interplanar carbon bonds of the pristine graphite and the formation of graphene nanosheets. Fig. S-2(a) shows the XRD pattern of pure graphene nanosheets, as a confirmation of the graphene in composite material. In the Raman spectrum (Fig. 1(b)), two typical Raman peaks of carbon, the D line and G line as shown, are observed at 1333 cm^{-1} and 1598 cm^{-1}, respectively, which are consistent with the Raman spectrum of pure graphene nanosheets (Fig.S-2(b)). The D line is stronger than the G line, and the D/G intensity ratio in the spectrum is significantly larger than that of well-crystallized graphite, indicating the decrease in the sp^2 carbon matrix of pristine graphite and the exfoliation of graphene layers [37]. As the intensity of the D line and the G line is quite high, only three other Raman peaks are clearly visible. These three peaks are located at 182 cm^{-1}, 470 cm^{-1}, and 658 cm^{-1}, respectively, and can be assigned to the F_{2g}, E_g, and A_{1g} active modes of the Co_3O_4 nanoparticles. The frequencies of these three Raman peaks are similar to that found in the standard microcrystalline Co_3O_4 powders [38].

The morphology of the nanocomposite material was observed by FESEM in general beam-high resolution (GB-HR) mode. The acquired FESEM image (Fig. 2(a)) at a low magnification exhibits numerous of graphene nanosheets in a curly and corrugated states. At a higher magnification (Fig. 2(b)), Co_3O_4 nanoparticles, with a size of ~20 nm, can be found to distribute densely and homogeneously on the surfaces of graphene nanosheets. We also observed the insertion of Co_3O_4 nanoparticles between the interlayers of the graphene nanosheets (as shown in Fig. 2(b)), and this confirms the presence of the sandwich-like architecture of the composite. The crystal structure of the Co_3O_4/graphene nanocomposite material was further examined by TEM analysis. Fig. 3(a) shows a low magnification TEM image, in which Co_3O_4 nanoparticles are clearly visible and dispersed homogenously on the graphene nanosheets. As the graphene nanosheets are corrugated in nature, some regions appeared darker, and the Co_3O_4 nanoparticles therefore appeared to be very close to each other, however, were actually isolated by different layers of graphene nanosheets. The particle sizes of these Co_3O_4 nanoparticles were determined to be 15–25 nm, which is consistent with the results of FESEM observation. The inset in Fig. 3(a) shows a selected area electron diffraction (SAED) pattern within this examined area. The diffraction rings from inside to outside were indexed to (2 2 0), (3 1 1), (4 0 0), (5 1 1), (4 4 0), and (5 3 3) planes of Co_3O_4 nanoparticles, respectively. A high resolution TEM (HRTEM) image focusing on a single Co_3O_4 nanoparticle is shown in Fig. 3(b). Crystal fringes were clearly displayed, and the *d*-spacing of this Co_3O_4 nanoparticle was derived to be 0.29 nm, corresponding to the spacing between (2 2 0) planes of nanocrystalline Co_3O_4.

AFM images (Fig. 4) within a 400 nm by 400 nm area reveal surface traces of graphene nanosheets and Co_3O_4 nanoparticles. As shown in Fig. 4(a), Co_3O_4 nanoparticles are identified as bright dots. From the view of height differences, it clearly shows that some of the Co_3O_4 nanoparticles were deposited on a lower layer of the graphene nanosheets, indicated by a lighter color above the red line. While others were dispersed on a relatively higher layer of graphene nanosheets, indicated by a brighter color below the red line. Graphene nanosheets were stacked in several layers and were corrugated when they were dried, resulting in height differences in the various areas examined. The Co_3O_4 nanoparticles stabilized the graphene nanosheets and acted as spacers to prevent the graphene layers from aggregation. The Co_3O_4 nanoparticles deposited at different height levels, as shown in this AFM image. Fig. 4(b) presents a height profile across the examined region, as marked by the red line in Fig. 4(a). The height difference of the single Co_3O_4 nanoparticle on the line is 17.8 nm, which is the size of the particle. The thickness of the graphene nanosheets lying on the line is evaluated to be 3–5 nm, which further confirmed the formation of several layers of graphene nanosheets. The weight percentage of the graphene nanosheets in Co_3O_4/graphene nanocomposite was determined by TGA measurement (as shown in Fig. S-3, SI). The dramatic weight loss was due to the decomposition of Co_3O_4 to CoO and the consumption of graphene in air as temperature increased. The final product left was CoO only with a weight percent of ~51.0%. The composition of Co_3O_4 nanoparticles in the Co_3O_4/graphene nanocomposite was determined to be 45.4 wt% based on the weight percentage of CoO. Therefore, the nanocomposite consists of 45.4 wt% graphene and 54.6 wt% Co_3O_4 nanoparticles.

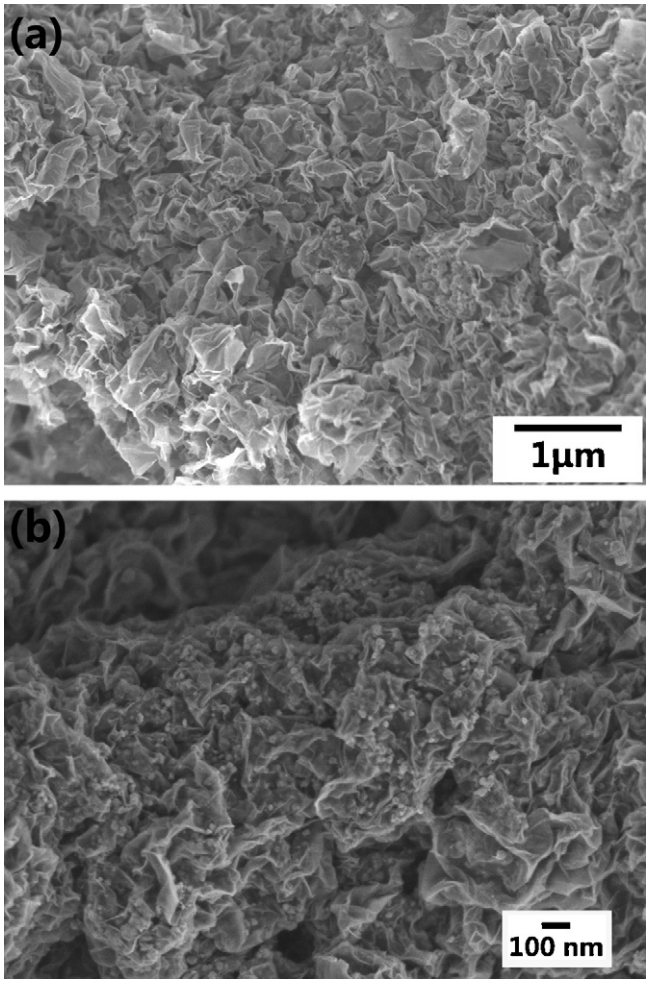

Fig. 2. FESEM images obtained under GB-HR mode: (a) numerous curly graphene nanosheets observed at a low magnification, and (b) a higher magnification image, displaying the distribution of Co_3O_4 nanoparticles on graphene nanosheets. The embedded Co_3O_4 nanoparticles are ~20 nm in size.

The electrochemical reactivity of Co_3O_4/graphene nanocomposite as anode material in lithium ion cells was first assessed by CV measurements. Fig. 5 shows the CV curves of Co_3O_4/graphene electrode in the first, second, and 50th scanning cycles. The redox reactions involved between Co_3O_4 and Li can be expressed as follows:

$$8Li^+ + Co_3O_4 + 8e^{-1} \leftrightarrow 4Li_2O + 3Co$$

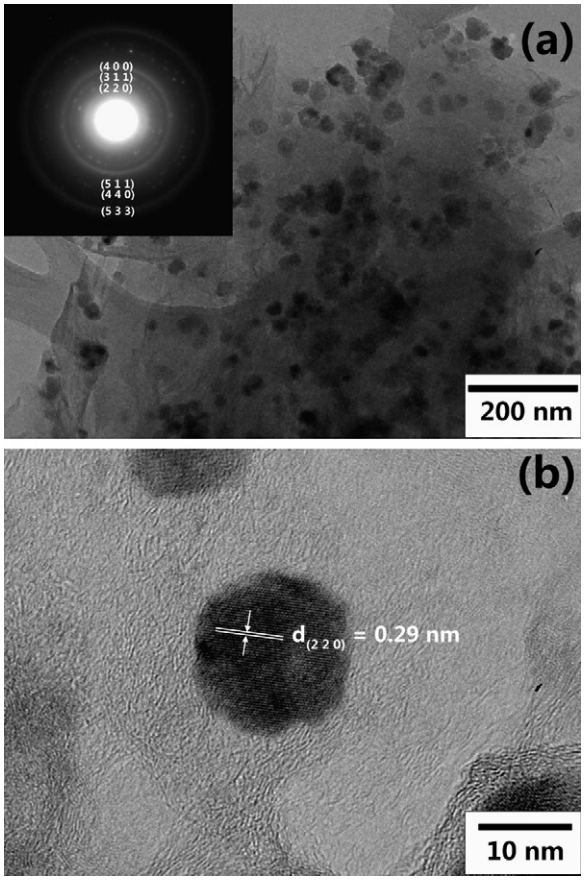

Fig. 3. TEM images of the Co_3O_4/graphene nanocomposite material: (a) a low magnification image showing Co_3O_4 nanoparticles dispersed on graphene nanosheets; (inset) the SAED pattern within this examined region; (b) an HRTEM image focusing on a single Co_3O_4 nanoparticle.

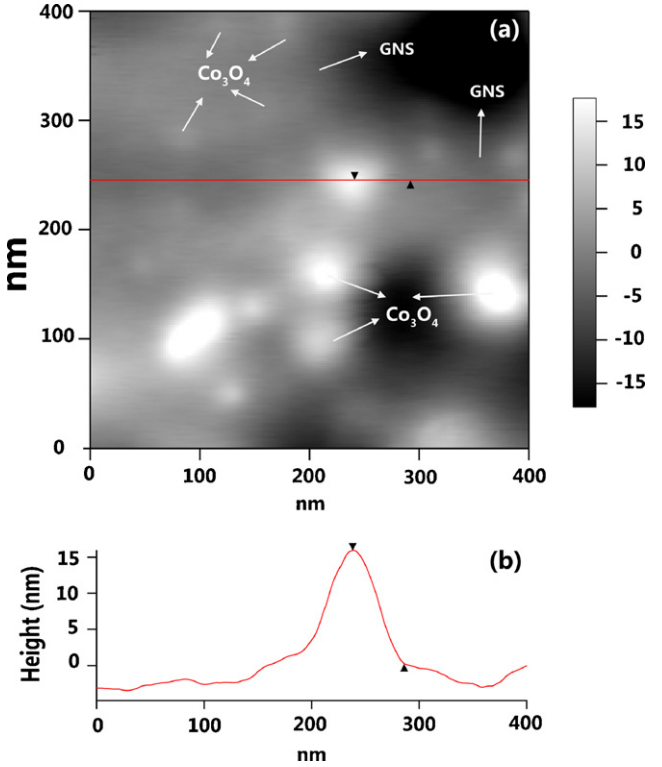

Fig. 4. AFM images covering an area of 400 nm by 400 nm: (a) surface evidence of graphene nanosheets and deposited Co_3O_4 nanoparticles; (b) height profile across the red line; the particle size of the single Co_3O_4 nanoparticle on the line is 17.8 nm. (For interpretation of the references to color in this figure legend, the reader is referred to the web version of this article.)

In the first cycle, the discharge curve has a longer sloping part, and two small cathodic peaks appear at 0.62 V and 0.84 V, which can be attributed to the formation of the solid electrolyte interphase (SEI) layer. Both of the peaks disappear from the second cycle. The other two reduction peaks are located around 0.6 V and 1.35 V, and could be due to the insertion of lithium ions into Co_3O_4 nanoparticles at different stages. Two oxidation peaks appear around 1.32 V and 2.2 V, and could be due to the process of lithium ion extraction from the Co_3O_4 nanoparticles. The insertion and extraction processes of lithium ions through graphene nanosheets are evidenced by the reduction and oxidation peaks located at 0.01 V and 0.17 V, respectively.

Fig. 6 shows the charge/discharge profile of the Co_3O_4/graphene nanocomposite material as anode in a lithium cell under galvanostatic charge/discharge cycling at a current of 55 mA. In the first cycle, the Co_3O_4/graphene nanocomposite material delivered a lithium insertion capacity of 1433 mAh g^{-1} and a reversible charge capacity of 705 mAh g^{-1}. In the second cycle, a discharge capacity of 722 mAh g^{-1} was obtained, while the reversibility was improved significantly and the composite electrode maintained a good cyclability. The theoretical capacity of lithium storage that graphene could contribute is 744 mAh g^{-1}, based on the assumption that all graphene nanosheets are well separated and strictly monolayers. On the other hand, Co_3O_4 should have a theoretical lithium capacity of 890 mAh g^{-1}. Our Co_3O_4/graphene nanocomposite material contains 54.6 wt% of Co_3O_4 nanoparticles and 45.4 wt% of graphene nanosheets. Therefore, the possible maximum theoretical capacity of the Co_3O_4/graphene nanocomposite material is calculated to be 823.7 mAh g^{-1}, based on the theoretical capacities of graphene (744 mAh g^{-1}) and Co_3O_4. It clearly shows that the initial reversible discharge capacity, 722 mAh g^{-1}, is very close to the theoretical capacity of the Co_3O_4/graphene nanocomposite material.

The reversible lithium storage capacity vs. cycle number of Co_3O_4/graphene, commercial Co_3O_4 nanoparticles and bare graphene nanosheets is shown in Fig. 7. The Co_3O_4/graphene electrode delivered a reversible discharge capacity of 722 mAh g^{-1} at 55 mA and maintained a capacity of 631 mAh g^{-1} after 50 cycles. On the other hand, the Co_3O_4 nanoparticle electrode exhibited better lithium storage capacity at the first few cycles and then faded quickly during the cycling test. Only 230 mAh g^{-1} was maintained after 50 cycles. The bare graphene electrode only exhibited a dis-

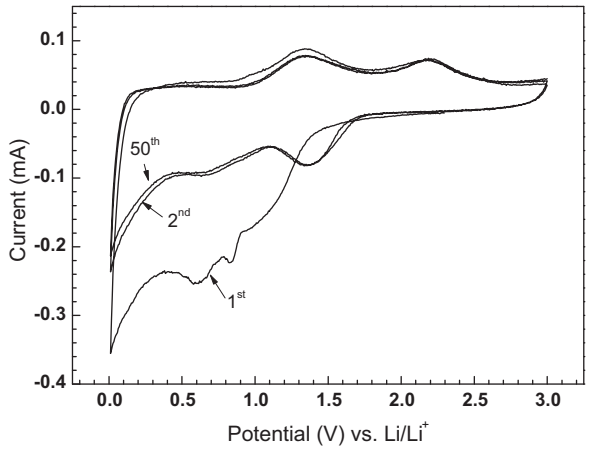

Fig. 5. CV curves of Co_3O_4/graphene anode over a voltage range of 0.01–3 V at a scan rate of 0.1 mV s^{-1} in the 1st, 2nd and 50th cycles.

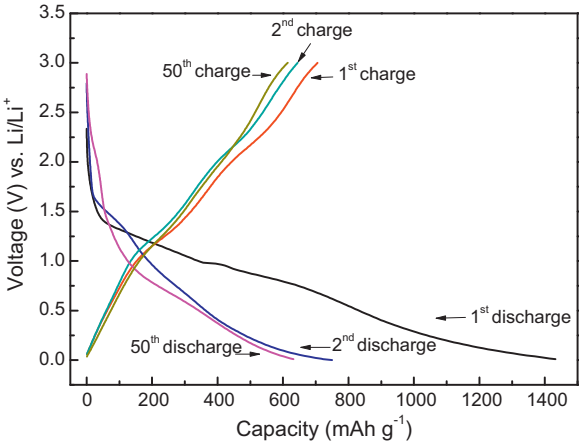

Fig. 6. Charge/discharge profiles of Co_3O_4/graphene anode at a current of 55 mA in the 1st, 2nd and 50th cycles.

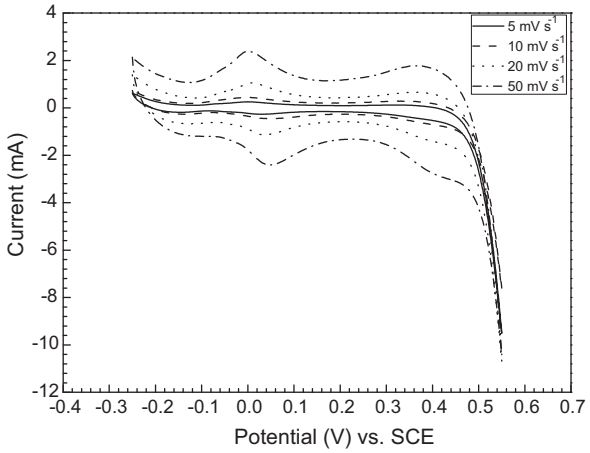

Fig. 8. CV curves of Co_3O_4/graphene as working electrode in a supercapacitor cell in 2 M KOH over a voltage range of −0.25 to 0.55 V at scan rates of 5 mV s^{-1}, 10 mV s^{-1}, 20 mV s^{-1}, and 50 mV s^{-1}, respectively.

charge capacity of 273 mAh g^{-1} after 50 cycles and 255 mAh g^{-1} after 100 cycles at 55 mA, as demonstrated in our previous studies [22]. Therefore, it has been shown that the Co_3O_4/graphene electrode performed much better than the bare graphene electrode or the Co_3O_4 nanoparticle electrode, by exhibiting highly reversible lithium storage capacity, excellent cycling stability, and high Columbic efficiency. The enhancement of the electrochemical properties, compared to bare graphene and Co_3O_4 nanoparticles, can be attributed to the contributions of both the graphene nanosheets and the Co_3O_4 nanoparticles. The distribution of Co_3O_4 nanoparticles among the graphene nanosheets has effectively separated these graphene nanosheets into uniformly layered structure and increased their lithium storage capacity. The graphene nanosheets in this case have provided carbons as a buffer medium to overcome the problem associated with the volume expansion/contraction in the lithium cells when Co_3O_4 nanoparticles react with lithium by lithium insertion/extraction [15,16]. Furthermore, the aggregation of Co_3O_4 nanoparticles on the graphene nanosheets can be efficiently prevented. Therefore, upon cycling, the active material can resist cracking and crumbling, and maintain large capacity and cycling stability [15]. As graphene has good conductivity [39], the internal resistance in the lithium cells could be minimized to stabilize the electronic and ionic conductivity, thereby leading to a higher specific capacity [40].

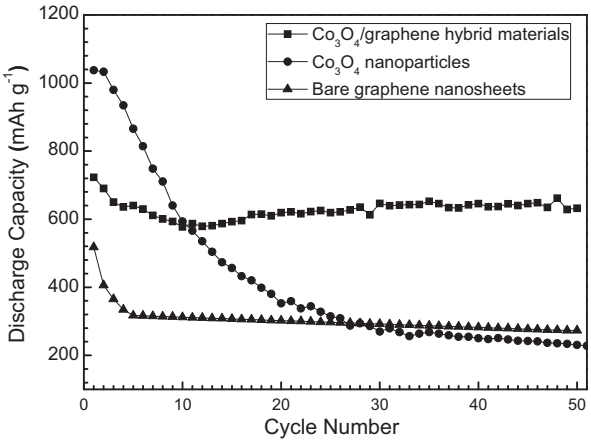

Fig. 7. Cycling performance of Co_3O_4/graphene nanocomposite material, Co_3O_4 nanoparticles, and bare graphene nanosheets as anode materials at a current of 55 mA.

Fig. 8 shows the CV curves of the as-prepared Co_3O_4/graphene nanocomposite material as electrode material in supercapacitor in 2 M KOH electrolyte at different scanning rates. All the CV curves present a similar shape with oxidation and reduction peaks at various scan rates. The oxidation peak at 0.36 V and the reduction peak at 0.42 V were assigned to the redox reactions arising from the embedded Co_3O_4 nanoparticles in 2 M KOH. In the lower voltage region, the −0.01 V oxidation peak and the 0.04 V reduction peak are due to the effects of epoxyl, hydroxyl, and carboxyl functional groups attached to the graphene nanosheets. These functional groups formed in the chemical synthesis process of graphene nanosheets [35,37]. The indirect evidence for these surface functional groups in the graphene-based composites was confirmed by us, by elemental analysis in our previous studies [26]. The maximum specific capacitance evaluated is 478 F g^{-1} at a scan rate of 5 mV s^{-1}. It is considered that double layer capacitance is generated by the graphene, while Co_3O_4 nanoparticles contribute pseudocapacitance from redox reactions to the total specific capacitance. Nanosized commercial Co_3O_4 powders (<50 nm) and bare graphene nanosheets yield a maximum specific capacitance of 118 F g^{-1} and 245 F g^{-1}, respectively, at 5 mV s^{-1} in 2 M KOH (Fig. S-4). Compared to the specific capacitance delivered by commercial Co_3O_4 nanoparticles and bare graphene nanosheets, the electrochemical performance of the Co_3O_4/graphene composite material is significantly increased as Co_3O_4 nanoparticles are inserted into graphene nanosheets. The presence of the Co_3O_4 nanoparticles prevents the graphene nanosheets from aggregation, making both sides of the graphene nanosheets accessible for K^+ ion insertion and de-insertion. Graphene nanosheets also provide highly conductive carbon matrix to minimize the internal resistance and facilitate the electrochemical activities. As bare graphene nanosheets are in the form of multi-layers, the BET surface area of graphene is only 93.7 m^2 g^{-1} and not sufficiently extended [26]. However, on the other hand, the BET surface area of our Co_3O_4/graphene composite material obtained from the N_2 adsorption/desorption isotherms in Fig. S-5, is dramatically extended to 219.2 m^2 g^{-1} due to the function of Co_3O_4 nanoparticles as spacers. The extended graphene layers, with enlarged interlayer space and surface area, are therefore favorable for the formation of double layer capacitance. Furthermore, the particle size of Co_3O_4 in graphene domain is restricted upon formation between graphene layers and is relatively smaller (15–25 nm), compared to commercial Co_3O_4 nanoparticles (<50 nm). The superior electrochemical behavior of the composite material is also associated with these smaller embedded nanoparticles. The decrease of the particle size

of the deposited Co_3O_4 nanoparticles would lead to the increase of the specific capacitance of those nanoparticles in the composite. Similar effect has been reported for composites having particles of RuO_2 deposited on carbon nanofibres [41]. It is also very interesting to find that the surface-related capacitance of the composite material is 2.18 F m^{-2}. This result is relatively larger than ordinary carbon [42], however, similar to those of carbon materials with surface functionalities [43,44]. It was proposed that surface functional groups attached to the carbon materials could provide supplementary pseudocapacitive contribution to a dominant double-layer capacitance to enhance the specific capacitance of the modified carbon materials [45–48]. Therefore, we believe the functional groups in our nanocomposite material are also electrochemical active, and could participate in the redox reactions and contribute extra pseudocapacitance to the electrochemical performance.

In summary, Co_3O_4 nanoparticles play two major roles in the Co_3O_4/graphene nanocomposite material in managing the enhancement of the electrochemical performance of the composite material. Firstly, the Co_3O_4 nanoparticles act as spacers to stabilize the graphene nanosheets. The interlayer space and accessible surface area of the graphene are therefore extended when Co_3O_4 nanoparticles are inserted. When applied in lithium-ion batteries and supercapacitors, graphene provides a highly conductive medium and much more flexible layers with enlarged interlayer space and increased surface area, benefiting the electrochemical performance in energy storage. Secondly, Co_3O_4 nanoparticles participate in the electrochemical activities, not only in lithium-ion batteries, but also in the supercapacitors. Co_3O_4 nanoparticles can deliver a high lithium-ion storage capacity and pseudocapacitance from redox reactions, and therefore make electrochemical contributions towards the overall electrochemical performance of the composite material.

4. Conclusions

An *in situ* chemical method has been developed to prepare Co_3O_4/graphene nanocomposite material for energy storage application. The prepared composite material consists of uniform Co_3O_4 nanoparticles (15–25 nm in size) distributed on separated graphene nanosheets. The electrochemical properties of the composite material are enhanced significantly, as embedded Co_3O_4 nanoparticles can protect graphene from aggregation. Co_3O_4/graphene nanocomposite material exhibited a high lithium storage capacity of 722 mAh g^{-1} in lithium-ion cells and a high supercapacitance of 478 F g^{-1} in supercapacitors.

Acknowledgements

We thank the Australian Research Council (ARC) for financial support through the ARC Discovery Project (DP1093855) and the ARC Linkage Project (LP0989134). We would also like to acknowledge the support from the National Foundation of Korea through a World Class University (WCU) Program (R32-2008-000-20093-0). Assoc. Prof. Alison Ung is highly appreciated for proofreading of the manuscript.

Appendix A. Supplementary data

Supplementary data associated with this article can be found, in the online version, at doi:10.1016/j.jallcom.2011.04.152.

References

[1] K.S. Novoselov, D. Jiang, F. Schedin, T.J. Booth, V.V. Khotkevich, S.V. Morozov, A.K. Geim, Proc. Natl. Acad. Sci. U.S.A. 102 (2005) 10451–10453.
[2] A.K. Geim, K.S. Novoselov, Nat. Mater. 6 (2007) 183–191.
[3] S. Stankovich, D.A. Dikin, G.H.B. Dommett, K.M. Kohlhaas, E.J. Zimney, E.A. Stach, R. Piner, S.T. Nguyen, R.S. Ruoff, Nature 442 (2006) 282–286.
[4] W.S. Hummers, R.E. Offeman, J. Am. Chem. Soc. 80 (1958) 1339.
[5] K.S. Kim, Y. Zhao, H. Jang, S.Y. Lee, J.M. Kim, K.S. Kim, J.-H. Ahn, P. Kim, J.-Y. Choi, B.H. Hong, Nature 457 (2009) 706–710.
[6] A. Dato, V. Radmilovic, Z. Lee, J. Phillips, M. Frenklach, Nano Lett. 8 (2008) 2012–2016.
[7] H.J. Park, J. Meyer, S. Roth, V. Skákalová, Carbon 48 (2010) 1088–1094.
[8] G.X. Wang, B. Wang, J. Park, Y. Wang, B. Sun, J. Yao, Carbon 47 (2009) 3242–3246.
[9] M. Choucair, P. Thordarson, J.A. Stride, Nat. Nanotech. 4 (2009) 30–33.
[10] M. Lotya, Y. Hernandez, P.J. King, R.J. Smith, V. Nicolosi, L.S. Karlsson, F.M. Blighe, S. De, Z. Wang, I.T. McGovern, G.S. Duesberg, J.N. Coleman, J. Am. Chem. Soc. 131 (2009) 3611–3620.
[11] G.X. Wang, X.P. Shen, J. Yao, J. Park, Carbon 47 (2009) 2049–2053.
[12] P. Guo, H. Song, X. Chen, Electrochem. Commun. 11 (2009) 1320–1324.
[13] E.J. Yoo, J. Kim, E. Hosono, H.S. Zhou, T. Kudo, I. Honma, Nano Lett. 8 (2008) 2277–2282.
[14] M.D. Stoller, S. Park, Y. Zhu, J. An, S.R. Ruoff, Nano Lett. 8 (2008) 3498–3502.
[15] S.-M. Paek, E.J. Yoo, I. Honma, Nano Lett. 9 (2009) 72–75.
[16] J. Yao, X.P. Shen, B. Wang, H. Liu, G.X. Wang, Electrochem. Commun. 11 (2009) 1849–1852.
[17] C. Xu, X. Wang, L. Yang, Y. Wu, J. Solid State Chem. 182 (2009) 2486–2490.
[18] Y. Si, E.T. Samulski, Chem. Mater. 20 (2008) 6792–6797.
[19] T. Lu, L.K. Pan, H.B. Li, G. Zhu, T. Lv, X.J. Liu, Z. Sun, T. Chen, D.H.C. Chua, J. Alloys Compd. 509 (2011) 5488–5492.
[20] R. Muszynski, B. Seger, P.V. Kamat, J. Phys. Chem. C 112 (2008) 5263–5266.
[21] L. Dong, R.R.S. Gari, Z. Li, M.M. Craig, S. Hou, Carbon 48 (2010) 781–787.
[22] G.X. Wang, B. Wang, X.L. Wang, J. Park, S.X. Dou, H. Ahn, K. Kim, J. Mater. Chem. 19 (2009) 8378–8384.
[23] H.F. Xiang, K. Zhang, G. Ji, J.Y. Lee, C.J. Zhou, X.D. Chen, J.S. Wu, Carbon 49 (2011) 1787–1796.
[24] B.J. Li, H.Q. Cao, J. Shao, M.Z. Qu, J.H. Warner, J. Mater. Chem. 21 (2011) 5069–5075.
[25] D.H. Wang, D.W. Choi, J. Li, Z.G. Yang, Z.M. Nie, R. Kou, D.H. Hu, L.V. Saraf, J.G. Zhang, I.A. Aksay, J. Liu, ACS Nano 3 (2009) 907–914.
[26] B. Wang, J. Park, C. Wang, H. Ahn, G. Wang, Electrochim. Acta 55 (2010) 6812–6817.
[27] X.W. Lou, D. Deng, J.Y. Lee, J. Feng, L.A. Archer, Adv. Mater. 20 (2008) 258–262.
[28] S.L. Xiong, C.Z. Yuan, M.F. Zhang, B.J. Xi, Y.T. Qian, Chem. Eur. J. 15 (2009) 5320–5326.
[29] J. Ma, S.P. Zhang, W. Liu, Y. Zhao, J. Alloys Compd. 490 (2010) 647–651.
[30] G.X. Wang, X.P. Shen, J. Horvat, B. Wang, H. Liu, D. Wexler, J. Yao, J. Phys. Chem. C 113 (2009) 4357–4361.
[31] L. Yang, W.S. Guan, B. Bai, Q. Xu, Y. Xiang, J. Alloys Compd. 504 (2010) L10–L13.
[32] G.X. Wang, X.P. Shen, J. Yao, D. Wexler, J.-H. Ahn, Electrochem. Commun. 11 (2009) 546–549.
[33] Y. Shan, L. Gao, Mater. Chem. Phys. 103 (2007) 206–210.
[34] Z.S. Wu, W. Ren, L. Wen, L. Gao, J. Zhao, Z. Chen, G. Zhou, F. Li, H.M. Cheng, ACS Nano 4 (2010) 3187–3194.
[35] N.I. Kovtyukhova, P.J. Oliver, B.R. Martin, T.E. Mallouk, S.A. Chizhik, E.V. Buzaneva, A.D. Gorchinskiy, Chem. Mater. 11 (1999) 771–778.
[36] D. Li, M.B. Müller, S. Gilje, R.B. Kaner, G.G. Wallace, Nat. Nanotech. 3 (2008) 101–105.
[37] S. Stankovich, D.A. Dikin, R.D. Piner, K.A. Kohlhaas, A. Kleinhammes, Y. Jia, Y. Wu, S.T. Nguyen, R.S. Ruoff, Carbon 45 (2007) 1558–1565.
[38] V.G. Hadjiev, M.N. Iliev, I.V. Vergilov, J. Phys. C: Solid State Phys. 21 (1988) L199–201.
[39] Z.S. Wu, W. Ren, L. Gao, B. Liu, C. Jiang, H.M. Cheng, Carbon 47 (2009) 493–499.
[40] C.H. Jiang, E. Hosono, H.S. Zhou, Nano Today 1 (2006) 28–33.
[41] F. Pico, J. Ibañez, M.A. Lillo-Rodenas, A. Linares-Solano, R.M. Rojas, J.M. Amarilla, J.M. Rojo, J. Power Sources 176 (2008) 417–425.
[42] K. Xia, Q. Gao, J. Jiang, J. Hu, Carbon 46 (2008) 1718–1726.
[43] D. Hulicova, J. Yamashita, Y. Soneda, H. Hatori, M. Kodama, Chem. Mater. 17 (2005) 1241–1247.
[44] D. Hulicova, M. Kodama, H. Hatori, Chem. Mater. 18 (2006) 2318–2326.
[45] E. Raymundo-Piñero, F. Leroux, F. Béguin, Adv. Mater. 18 (2006) 1877–1882.
[46] F. Béguin, K. Szostak, G. Lota, E. Frackowiak, Adv. Mater. 17 (2005) 2380–2384.
[47] D. Hulicova, M. Kodama, S. Shiraishi, H. Hatori, Z.H. Zhu, G.Q. Lu, Adv. Funct. Mater. 19 (2009) 1800–1809.
[48] E. Frackowiak, G. Lota, J. Machnikowski, C. Vix-Guterl, F. Béguin, Electrochim. Acta 51 (2006) 2209–2214.